



Harmonizing Landsat 8 and Sentinel-2: A time-series-based reflectance adjustment approach

Rong Shang^{*}, Zhe Zhu

Department of Natural Resources and the Environment, University of Connecticut, Storrs, CT, 06269, United States

ARTICLE INFO

Keywords:

Landsat 8
Sentinel-2
Spectral response function
Reflectance difference
Consistency
Reflectance adjustment
TRA

ABSTRACT

We developed a Time-series-based Reflectance Adjustment (TRA) approach for reducing the reflectance differences between Landsat 8 and Sentinel-2 observations. This TRA approach used the time series of matched Landsat 8 and Sentinel-2 observations to build linear regression models to adjust reflectance differences between the two sensors for each individual pixel and each spectral band. We evaluated this approach for the NASA harmonized Landsat and Sentinel-2 (HLS) surface reflectance product (V1.4; <https://hls.gsfc.nasa.gov/data/v1.4/>) and top-of-atmosphere (TOA) reflectance with approximately 4 years of temporal coverage at five Military Grid Reference System (MGRS) tiles. Using this approach, the surface reflectance difference between Landsat 8 and Sentinel-2 in the HLS product reduced 45% for the blue band, 42% for the green band, 38% for the red band, 30% for the Near Infrared (NIR) band, 37% for the Shortwave Infrared (SWIR) 1 band, and 32% for the SWIR2 band. The TRA approach also reduced TOA reflectance difference between Landsat 8 and Sentinel-2 substantially, in which the blue band reduced 46%, the green and NIR bands reduced 42%, the red band reduced 48%, and the SWIR1 and SWIR2 bands reduced 44%. If the high aerosol observations were screened, the reflectance differences in the HLS product could be further reduced by 2–4% and the TOA reflectance differences could be further reduced by 3–6% for the six spectral bands. The TRA approach has also shown good results in reserving the spatial patterns and the heterogeneity of land surface. The transformation parameters estimated from the TRA approach can be directly used for future Landsat 8 and Sentinel-2 reflectance adjustment, with slightly lower (5%) reduction of reflectance difference.

1. Introduction

High temporal frequency Earth Observation (EO) satellites are pivotal for near real-time monitoring of land surface change (Zhu, 2017), such as vegetation anomaly and phenology change (Liu et al., 2018; Meroni et al., 2019), forest disturbance (Reiche et al., 2018; Tang et al., 2019; Xin et al., 2013), disaster (Li et al., 2018), surface water change (Pekel et al., 2014), and agriculture practices (Defourny et al., 2019). However, most of the satellites with high temporal frequency are coarse resolution satellites (250–1,000 m), such as Moderate Resolution Imaging Spectroradiometer (MODIS), Medium Resolution Imaging Spectrometer (MERIS), and Visible Infrared Imaging Radiometer Suite (VIIRS), which are not ideal for detecting land surface change that are usually occurring at a scale much smaller than their pixel sizes (Hansen and Loveland, 2012; Xin et al., 2013). On the other hand, moderate resolution satellites, such as Landsat, can provide observations at 30-m spatial resolution, which is fine enough to monitor a variety of landscape change (Roy et al., 2014; Wulder et al., 2019; Zhu et al., 2019),

but its temporal resolution is not sufficient for near real-time monitoring. For example, one Landsat satellite revisits the same location in every 16 days, which means even with two Landsat sensors working at the same time (e.g., Landsat 7 and 8), we can only visit the same place in every 8 days (assuming no cloud and snow cover). Fortunately, the recently launched Sentinel-2A and 2B have similar band designs as Landsat (Drusch et al., 2012), and they together need 5 days to repeat observations at 10–20–60 m spatial resolution, making it possible to observe global land surface in every 2–4 days when Landsat and Sentinel-2 satellites are combined (Li and Roy, 2017). Though Sentinel-2 can provide “Landsat-like” observations, they differ in the field of view, spatial resolution, spectral bandwidth, and spectral response function (Zhang et al., 2018). The difference introduced by different field of view and spatial resolution can be reduced and solved by the Bidirectional Reflectance Distribution Function (BRDF) correction (Kovalskyy et al., 2016) and data resampling, respectively. However, the difference caused by different spectral bandwidth and spectral response function (hereafter referred to as reflectance difference) remains a challenge for

^{*} Corresponding author.

E-mail address: rong.shang@uconn.edu (R. Shang).

<https://doi.org/10.1016/j.rse.2019.111439>

Received 9 March 2019; Received in revised form 20 September 2019; Accepted 21 September 2019

Available online 09 November 2019

0034-4257/ © 2019 Elsevier Inc. All rights reserved.

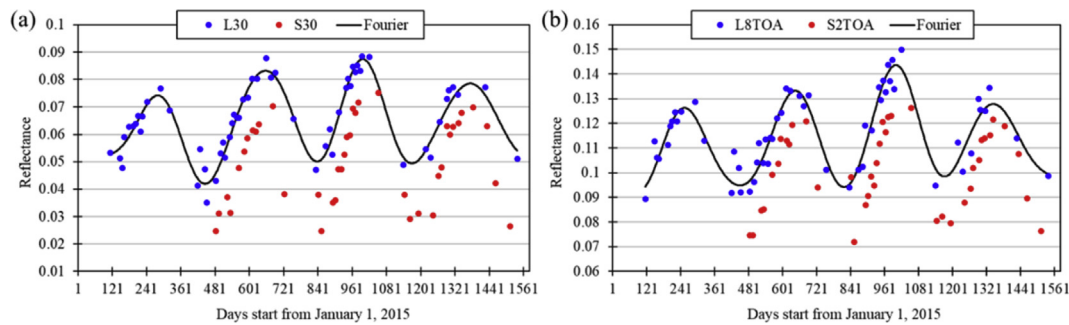


Fig. 1. An example of reflectance difference between L30 and S30 blue band surface reflectance derived from the HLS V1.4 products (a), and between L8TOA and S2TOA blue band top-of-atmosphere (TOA) reflectance (b). The black lines are the estimated curves of the L30 and L8TOA based on the Fourier approach (Dash et al., 2010) with 10 harmonics, respectively. The invalid observations (cloud, cloud shadow, and snow) were screened by the QA band in the HLS product. HLS: Harmonized Landsat and Sentinel-2 data product; L30: Landsat 8 data in the HLS product at 30-m resolution; S30: Sentinel-2 data in the HLS product at 30-m resolution; L8TOA: Landsat 8 TOA reflectance; S2TOA: the resampled Sentinel-2 TOA reflectance at 30-m resolution. (For interpretation of the references to color in this figure legend, the reader is referred to the Web version of this article.)

the remote sensing community.

The linear regression approach has been widely used to reduce the reflectance difference between the two similar satellite observations (Chastain et al., 2019; Claverie et al., 2018; Flood, 2017; Mandanici and Bitelli, 2016; Pahlevan et al., 2019; Zhang et al., 2018). For example, regional fixed per-band transformation coefficients were generated for reflectance adjustment in Australia (Flood, 2017), southern Africa (Zhang et al., 2018), and the conterminous United States (Chastain et al., 2019). Particularly, NASA Scientists proposed a method that creates global fixed per-band transformation coefficients to reduce the reflectance difference between Landsat 8 and Sentinel-2 for the harmonized Landsat and Sentinel-2 (HLS) surface reflectance product (Claverie et al., 2018). Though these methods can reduce reflectance difference to some degree, large reflectance differences were still observed (Fig. 1). Fig. 1a illustrates an example of the surface reflectance difference between the Landsat 8 (L30) and Sentinel-2 (S30) blue band surface reflectance in the HLS V1.4 product (hereafter referred to as HLS product). The average difference in the HLS product (0.0183) was 37% (average difference/average S30 \times 100%) of the magnitude of the average S30 surface reflectance. Significant reflectance difference was also observed between Landsat 8 and Sentinel-2 TOA reflectance, and the average TOA reflectance difference (0.0176) was 17% of the magnitude of the average Sentinel-2 TOA reflectance (Fig. 1b). It is possible that the regional or global scale fixed per-band transformation coefficients may not be suitable for all land cover types and at all locations (Chastain et al., 2019), consequently resulting in large differences between the harmonized Landsat 8 and Sentinel-2 surface reflectance. The time-series-based model, which can build the reflectance adjustment relationship for each pixel using the time series overlap of the two similar satellite observations, can be a better choice for harmonizing Landsat 8 and Sentinel-2 surface and TOA reflectance.

Here, we aim to improve the consistency of the Landsat 8 and Sentinel-2 surface (the HLS product) and TOA reflectance using a newly developed Time-series-based Reflectance Adjustment (TRA) approach. This time-series-based approach used the time series of matched Landsat 8 and Sentinel-2 observations to build linear regression models for each pixel and then conduct the reflectance adjustment for each individual pixel separately. We explored the optimal matching method for building the time-series-based model based on the HLS product at five sites and assessed the capability of the TRA approach for reserving the spatial patterns and the heterogeneity of land surface. The influences of high aerosol screening on the TRA adjustment of surface and TOA reflectance were also evaluated. Finally, we assessed whether the transformation parameters estimated from the TRA approach can be directly used for future Landsat and Sentinel-2 reflectance adjustment.

2. Data and methods

2.1. Data

The Harmonized Landsat and Sentinel-2 (HLS) V1.4 surface reflectance product (Claverie et al., 2018), which spans from January 2015 to April 2019 (approximately 4 years of temporal coverage for Sentinel-2A), was used to develop and evaluate the TRA approach. It provides consistent and harmonized 30-m surface reflectance derived from Landsat 8 (L30) and Sentinel-2 (S30) with the Military Grid Reference System (MGRS) in the Universal Transverse Mercator (UTM) projection. Four processes involved in the creation of this product: (i) atmospheric correction and cloud masking, (ii) geometric resampling and geographic registration, (iii) BRDF correction, and (iv) spectral bandwidth and spectral response function (or bandpass) adjustment (Claverie et al., 2018). This bandpass adjustment (hereafter referred to as HLS bandpass adjustment) used a linear regression model with fixed per-band regression coefficients to further reduce the reflectance difference between Landsat 8 and Sentinel-2 surface reflectance at the global scale (Claverie et al., 2018). Note that we did not use the HLS S30 surface reflectance directly. Instead, we used the BRDF-corrected Sentinel-2 surface reflectance from the first three steps (hereafter referred to as NadirS30), which was derived by reversing the HLS bandpass adjustment from the S30 surface reflectance based on the fixed per-band regression coefficients provided in the HLS product (Table 1). Three visible bands (Red, Green, and Blue), one near-infrared (NIR) band, and two shortwave infrared bands (SWIR1 and SWIR2) were chosen for reflectance adjustment here (The detailed band numbers of Landsat 8 and Sentinel-2 are shown in Table 1). The QA band in the HLS product provides information about cirrus, cloud, adjacent cloud, cloud shadow, snow/ice, water, and aerosol quality. The aerosol quality includes four levels: climatology, low, average and high. In this study, we masked out the cirrus, cloud, adjacent cloud, and cloud shadow pixels. The water and snow/ice pixels were also excluded to focus on land surface monitoring. Note that the aerosol quality was not

Table 1
Bandpass adjustment coefficients in the HLS V1.4 products.

Band Name	Landsat 8 band number	Sentinel-2 band number	Slope	Intercept
Blue	2	2	0.9778	-0.004
Green	3	3	1.0053	-0.0009
Red	4	4	0.9765	0.0009
NIR	5	8A	0.9983	-0.0001
SWIR1	6	11	0.9987	-0.0011
SWIR2	7	12	1.003	-0.0012

used to mask out the high aerosol pixels for building the reflectance adjustment relationship because the majority of pixels with thick aerosols were also identified by the cloud mask (Zhu and Woodcock, 2012), but the influence of high aerosols on reflectance adjustment would be evaluated. The GlobLand30 land cover product (Chen et al., 2015) was used to provide land cover information for all harmonized observations.

Landsat 8 and Sentinel-2 TOA reflectance were also used to evaluate the TRA approach. Google earth engine (GEE) was used to preprocess and download Landsat 8 and Sentinel-2 TOA reflectance (Gorelick et al., 2017). For Landsat 8, both Collection 1 Tier 1 (T1) and Tier 2 (T2) data were downloaded (hereafter referred to as L8TOA). We first re-projected the L8TOA to the projection of the HLS product and then clipped the L8TOA using the MGRS tile extent. For Sentinel-2, L1C data (hereafter referred to as S2TOA) were first resampled to 30-m spatial resolution and then downloaded through the MGRS tile. Red, green, and blue bands were resampled from 10-m spatial resolution, and NIR, SWIR1, and SWIR2 bands were resampled from 20-m spatial resolution. Resample in GEE was based on the overlap between the input and output images, and the input pixel weights were calculated as the ratio of the output pixel area covered by the input pixel. Note that cloud masks of the L8TOA and S2TOA were different from cloud masks in the HLS product. To keep consistency, we use the QA bands from the HLS product to label the quality of the L8TOA and S2TOA data instead of their own QA bands.

2.2. Study area

Five MGRS tiles (Fig. 2) were chosen for reflectance adjustment according to the land cover types, locations, and the quality of Landsat 8 and Sentinel-2 data (e.g., the frequency of cloud cover and aerosols). The DE site (Tile ID: 32UNA) and the TIF site (Tile ID: 17RKQ) were selected due to the frequent cloud cover. The DE site was mainly covered by cropland under the oceanic climate in Europe, while the TIF site was mainly covered by forest and cropland under the humid subtropical climate in North America. The SHA site (Tile ID: 50SMF) was chosen for its potential of high aerosols, and this site was mainly covered by the cropland with more than one growing season under the humid continental climate in China. The SEA site (Tile ID: 54JYP) was selected for

less cloud cover, and it mainly includes grassland and forest under the semi-arid climate in Australia. The TZ site (Tile ID: 36MWS) was mainly covered by forest and grassland under the tropical savanna climate in Africa, and it was selected for its frequent cloud cover in the wet season. The land cover map of the five tiles derived from the GlobLand30 land cover dataset (Chen et al., 2015) is shown in Fig. 3, and the percentages of invalid observations (cloud, cloud shadow, water, and snow) of the five sites are shown in Fig. S1.

2.3. Methods

The TRA approach establishes a reflectance adjustment relationship for each pixel and for each spectral band using matched Landsat 8 and Sentinel-2 observations. This approach had three major steps as follows (Fig. 4): (i) match Landsat 8 and Sentinel-2 observations; (ii) build reflectance adjustment relationship for each pixel and each spectral band; and (iii) reflectance adjustment for Sentinel-2 images. Note that for reflectance adjustment of the HLS data, we will apply the TRA approach for the HLS data without the HLS bandpass adjustment. Basically, we will reverse their reflectance adjustment to transfer S30 to NadirS30 using the linear regression model with the fixed per-band regression coefficients (Table 1).

2.3.1. Match Landsat 8 and Sentinel-2 observations

Ideally, we can have Landsat 8 and Sentinel-2 observations collected within the same date for building the reflectance adjustment relationship. However, in reality, the acquisition dates of Landsat 8 and Sentinel-2 are usually different, and it is almost impossible to collect enough clear-sky Landsat 8 and Sentinel-2 observations within the same date for building the reflectance adjustment relationship. Here, we assumed that data collected close in time should have similar values (Qiu et al., 2019; Zhu et al., 2010), and used Landsat 8 observation collected within ± 1 day of the Sentinel-2 acquisition date to match the Sentinel-2 observation (hereafter referred to as the one-day matching method). For example, if S30 is obtained on DOY (day-of-year) 120, then L30 obtained from DOY 119 to DOY 121 will be used to match NadirS30. In this way, many Sentinel-2 observations could be matched with a Landsat 8 observation, and there could be sufficient pairs of clear-sky Landsat 8 and Sentinel-2 observations collected to build the reflectance

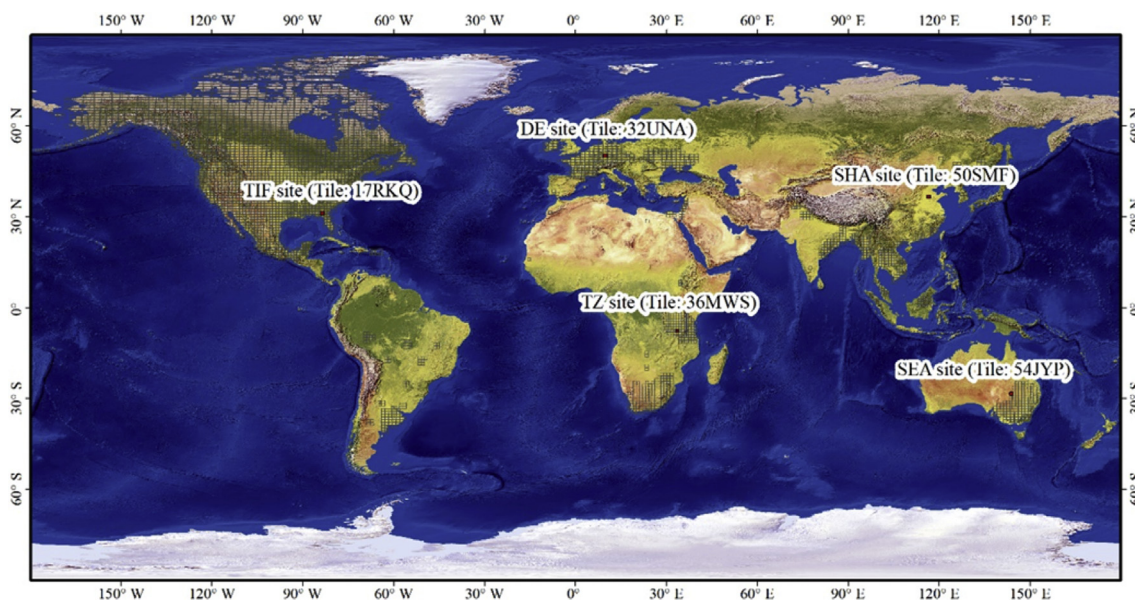


Fig. 2. Five MGRS tiles and their site names. The background is the 1:50 m Natural Earth I with Shaded Relief dataset (version 3.2.0; <https://www.naturalearthdata.com/>) and colors are based on land cover. The central location is (9.77°E, 50.05°N) for the DE site, (143.60°E, 28.49°S) for the SEA site, (116.49°E, 36.55°N) for the SHA site, (83.57°W, 31.11°N) for the TIF site, and (33.50°E, 7.73°S) for the TZ site. (For interpretation of the references to color in this figure legend, the reader is referred to the Web version of this article.)

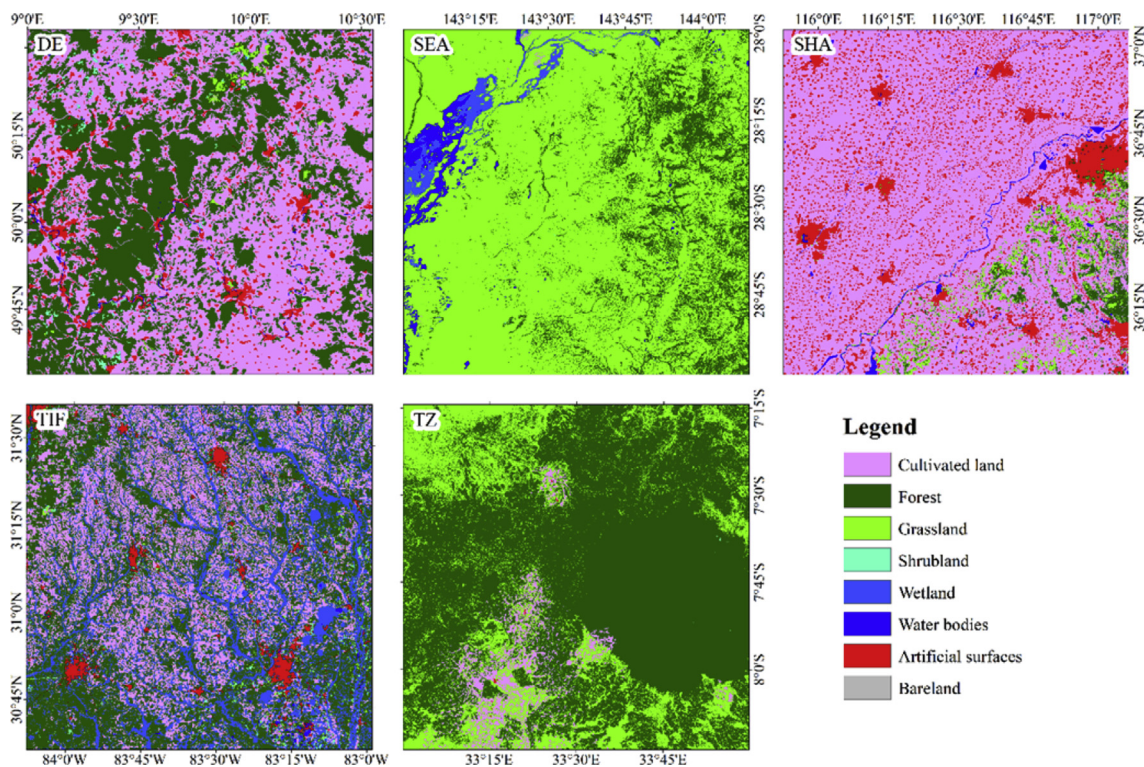


Fig. 3. Land cover maps derived from the GlobeLand30 land cover dataset (Chen et al., 2015) at the five sites.

adjustment relationship for 87.25% of pixels at the entire study area. We compared reflectance adjustment performances using different temporal windows (window size = 1, 2 and 3 days) to match L30 and NadirS30 (Fig. S2), and the optimum result was achieved when the window size was equal to ± 1 day (Fig. S2).

The current Sentinel-2 cloud mask used in the HLS product was a combination of the mask generated by the Fmask V3.3 algorithm (Zhu et al., 2015) and the mask derived from the LaSRC v3.5.5 atmospheric correction tool. This cloud mask would miss many cloud observations due to the lack of a thermal infrared band (Claverie et al., 2018), and some outlier filtering approaches are needed to screen these missed clouds. In this study, we adopted a filter designed by Zhang et al. (2018) to exclude cloud observations that were missed in the HLS QA band by comparing Landsat 8 and Sentinel-2 blue band reflectance:

$$|\rho_{\text{blue, Landsat 8}} - \rho_{\text{blue, Sentinel-2}}| > 0.5 \times |\rho_{\text{blue, Landsat 8}} + \rho_{\text{blue, Sentinel-2}}| \quad (1)$$

where, $\rho_{\text{blue, Landsat 8}}$ and $\rho_{\text{blue, Sentinel-2}}$ are the matched Landsat 8 and Sentinel-2 surface reflectance, respectively. This filter is designed based on the fact that the blue band is very sensitive to atmospheric influences (Ju et al., 2012) and the blue band reflectance of land surface is usually much lower than cloud and snow (Hagolle et al., 2010). The pairs of observations with one clear and one cloudy would be rejected, and some outliers due to “over correction” by LaSRC would also be screened (Zhang et al., 2018).

2.3.2. Build the reflectance adjustment relationship for each pixel

The linear regression model was used to build the reflectance adjustment relationship between Landsat 8 and Sentinel-2 surface reflectance for all the six bands (Eq. (2)):

$$y(\Lambda) = a(\Lambda) \times x(\Lambda) + b(\Lambda) \quad (2)$$

where, Λ is the band index, $x(\Lambda)$ is the NadirS30 surface reflectance, $y(\Lambda)$ is the L30 surface reflectance, and $a(\Lambda)$ and $b(\Lambda)$ are the estimated parameters. The estimated parameters for each pixel were obtained by minimizing the difference between the matched NadirS30 and L30

surface reflectance. As linear regression model without intercept ($y(\Lambda) = a(\Lambda) \times x(\Lambda)$) also demonstrated good performance in TOA reflectance calibration between MODIS and Landsat-7 data (Chander et al., 2013), we compared the performance of the linear regression model with and without intercept. Results showed that, without using the intercept, the reduced percentage of reflectance differences in the HLS product decreased 7% for the blue band, 4% for the green band, 3% for the red band, 5% for the NIR band, 2% for the SWIR1 band, and 3% for the SWIR2 band (Fig. S3), suggesting that linear regression model with intercept is a better option. For pixels with at least four pairs of matched clear-sky Landsat 8 and Sentinel-2 observations (hereafter referred to as Valid Pair of Observations, VPO), the reflectance adjustment relationship could be derived directly. But for pixels with frequent cloud covers, they may have less than four VPOs, and to adjust the reflectance for those pixels, we need to make full use of the unmatched clear-sky Landsat 8 and Sentinel-2 observations by using time series interpolation to match Sentinel-2 observations with interpolated Landsat 8 observations.

We evaluated five different time series interpolation approaches combined with three different matching methods to determine the optimal interpolation and matching methods. Five time series interpolation approaches included the linear interpolation (shortened to Linear), the locally adjusted cubic spline capping (LACC) approach (Chen et al., 2006), the Fourier approach (Dash et al., 2010), the Savitzky-Golay (SG) filter (Chen et al., 2004), and the iterative interpolation for data reconstruction (IDR) (Julien and Sobrino, 2010) were used to reconstruct daily L30 reflectance (hereafter referred to as InterpolateL30) based on all valid L30 reflectance. The three matching methods included (i) same-day matching method, which used InterpolateL30 within the same acquisition date of Sentinel-2 to match all NadirS30; (ii) one-day and interpolation matching method, which first used one-day matching method to match L30 and NadirS30, and then used same-day matching method to match InterpolateL30 and unmatched NadirS30; and (iii) one-day and valid interpolation matching method, which first used one-day matching method to match L30 and NadirS30, and then used same-day matching method to match “good

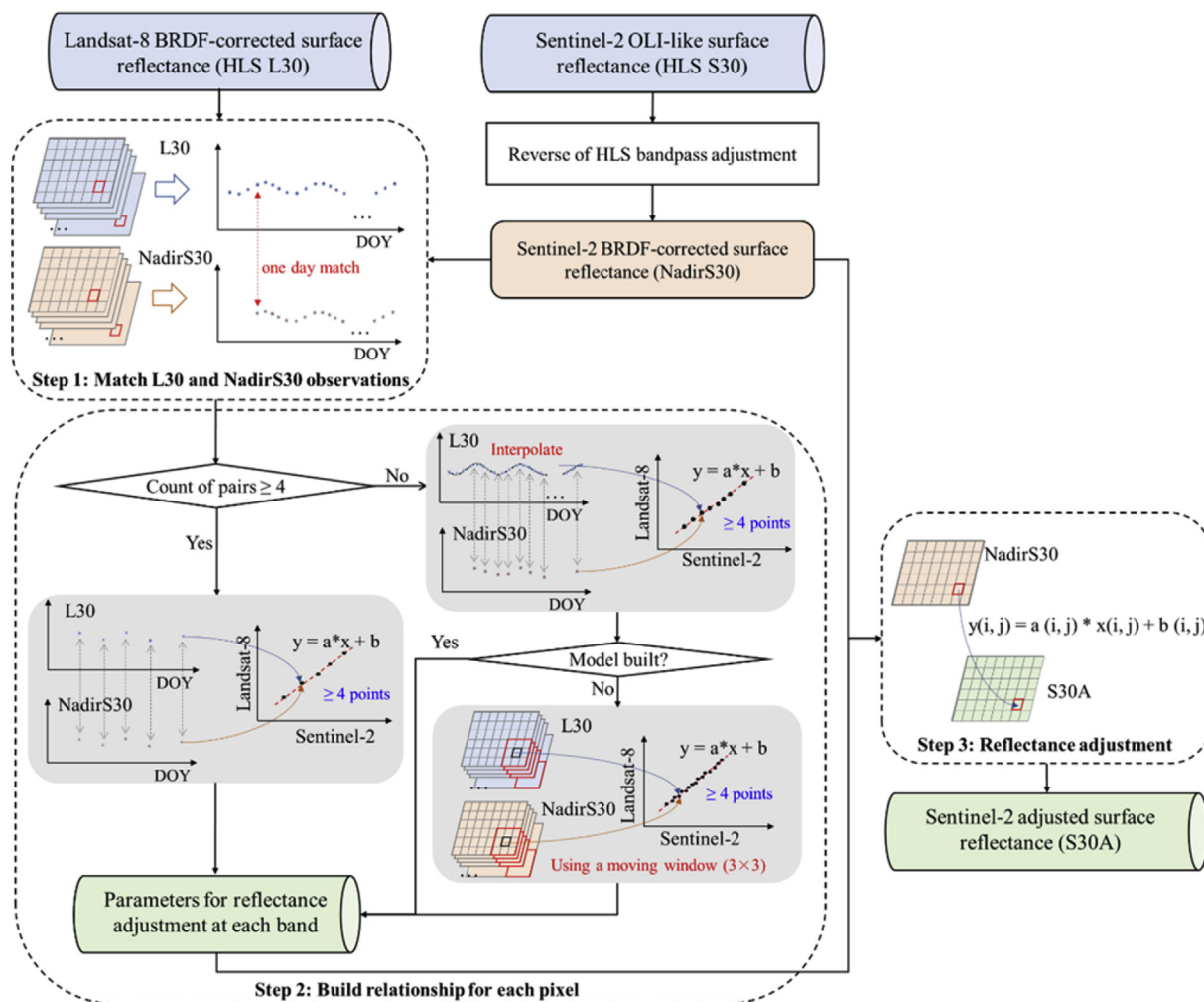


Fig. 4. Flowchart of the TRA approach applied to the HLS product.

quality” InterpolateL30 and unmatched NadirS30. The three different matching methods were created based on the assumption that actual observation is more accurate than the interpolated values and some of the interpolated values may have large errors due to the lack of available observations. The quality of an interpolated observation was labeled as “good” if there are valid L30 observations within ± 16 days (this threshold was determined from the Landsat-8 16-day revisit frequency); otherwise, it was labeled as “poor quality”. This quality assessment was conducted to minimize the influence of persistent cloud or snow covers which could cause an unreliable reconstruction for many time series interpolation approaches (Liu et al., 2017). Fig. S2 shows the performance of reflectance adjustment using 15 different kinds of approaches (3 matching methods \times 5 interpolating methods), in which the third matching method (one-day and valid interpolation matching method) showed the best results for all 5 interpolating methods. When using the third matching method, linear interpolation and the Fourier approach performed much better than the other three approaches, and they were also slightly better than the two-days and three-days matching methods. Since linear interpolation performed slightly better than the Fourier approach and it is more efficient, the third method with linear interpolation was selected as the optimal matching and interpolating method, and would be used for the pixels where there were less than 4 one-day matched VPOs. However, for some extreme cases, even the optimal matching and interpolating method may not have enough VPOs. Fig. 5 shows the spatial distribution of the number of VPOs using the one-day, two-days, three-days matching methods, and the optimal matching and interpolating method

proposed here. Though the optimal matching and interpolating method can work for 98.36% of pixels at the entire study area (the detailed percentage for each site are shown in Table S2), there are still pixels with less than four VPOs. For these pixels, a backup algorithm with a 3×3 spatial window would be applied. The reflectance adjustment relationship for these pixels would be built by using all VPOs within the 3×3 spatial window, and they would be labeled in their output QA.

2.3.3. Reflectance adjustment for Sentinel-2 observations

After the reflectance adjustment relationship was built for each pixel, the reflectance adjustment will be applied for each pixel using the previously built linear regression model. All the pixels in a Sentinel-2 image would be adjusted if the original reflectance and the adjusted reflectance values both ranged from 0 to 1. The output QA band of the adjusted Sentinel-2 image was set into 8 different values according to its input QA band and whether the backup algorithm was used: 1 (Clear), 2 (Clear but use the backup algorithm), 3 (Cloud), 4 (Cirrus), 5 (Shadow), 6 (Snow/ice), 7 (Water), and 255 (Filled value).

2.4. Evaluating TRA performance

The Root Mean Square Difference (RMSD) value was used as the indicator to quantitatively evaluate the reflectance difference between Landsat 8 and Sentinel-2 observations (Eq. (3)). The clear-sky Landsat 8 observations collected within ± 1 day of Sentinel-2 observations were used as the reference, and the RMSD was calculated based on the differences between Landsat 8 and Sentinel-2 reflectance for each pixel as

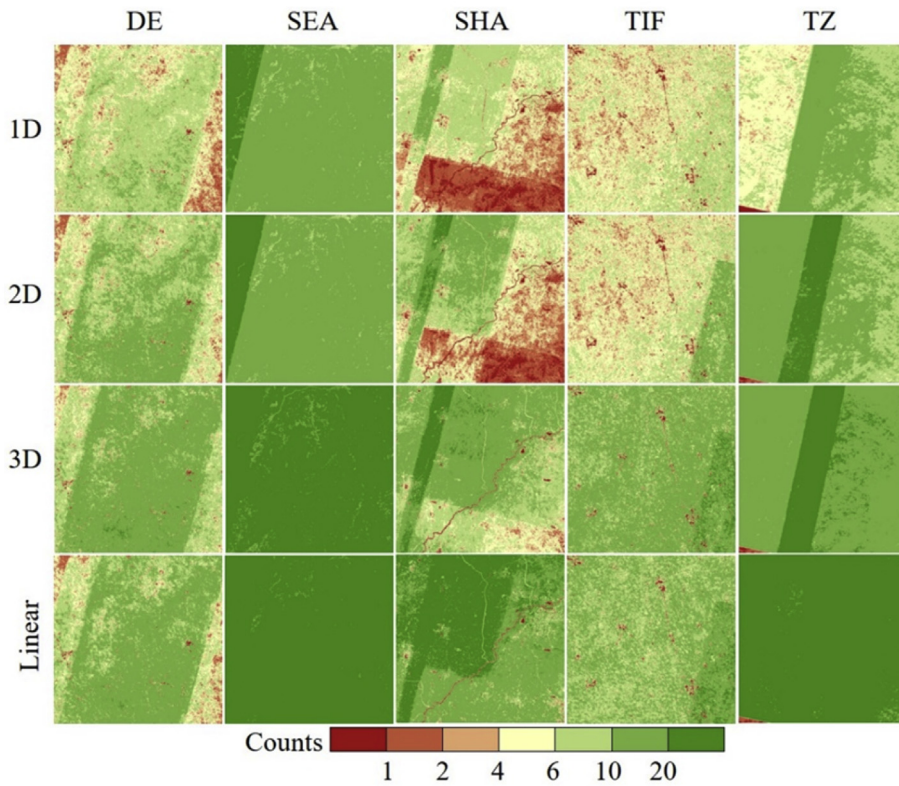


Fig. 5. The counts of valid pairs of observations (VPO) collected with the one-day (1D), two-days (2D), and three-days (3D) matching methods and the optimal (Linear) matching method for building the reflectance adjustment relationship at the five sites. The yellow and green colors (count of VPOs ≥ 4) work for the TRA approach. (For interpretation of the references to color in this figure legend, the reader is referred to the Web version of this article.)

	Blue	Green	Red	NIR	SWIR1	SWIR2
DE	96.27	73.72	86.31	258.27	202.11	143.41
SEA	74.45	93.66	130.45	141.80	227.64	179.10
SHA	86.51	96.16	104.85	159.01	162.62	141.25
TIF	75.36	62.99	74.17	203.57	211.50	150.88
TZ	54.02	53.07	60.51	126.25	144.38	100.27

(a) HLS surface reflectance before HLS bandpass adjustment

DE	99.48	74.84	86.18	257.99	197.75	141.41
SEA	80.82	96.65	119.10	141.51	221.15	178.73
SHA	94.49	98.09	105.06	159.68	157.02	138.92
TIF	74.90	63.51	74.22	202.97	205.92	147.55
TZ	58.05	55.29	60.22	126.51	138.38	98.29

(b) HLS surface reflectance after HLS bandpass adjustment

DE	137.91	123.14	146.53	409.14	292.13	204.12
SEA	94.61	101.60	201.77	239.83	346.59	281.70
SHA	147.82	120.78	145.39	228.36	227.35	205.59
TIF	122.69	120.97	143.31	341.86	321.45	236.10
TZ	101.75	89.69	116.19	206.20	222.67	166.92

(c) TOA reflectance

Fig. 6. The reflectance differences (expanded 10,000 times) between Landsat 8 and Sentinel-2 surface reflectance in the HLS product and TOA reflectance for six spectral bands at the five sites. (a) was calculated between L30 and NadirS30, (b) was calculated between L30 and S30, and (c) was calculated between Landsat 8 and Sentinel-2 TOA reflectance.

shown in Eq. (3):

$$RMSD(\Lambda) = \sqrt{\sum_i [\rho^{Landsat}(\Lambda, i) - \rho^{Sentinel}(\Lambda, i)]^2 / N} \quad (3)$$

where, Λ is the band index, $\rho^{Landsat}(\Lambda, i)$ is Landsat 8 reflectance, $\rho^{Sentinel}(\Lambda, i)$ is the original or adjusted Sentinel-2 reflectance, i is the i th pair of matched reflectance, and N is the total counts of matched reflectance. The mean RMSD for each tile, land cover type, and the entire

	Blue	Green	Red	NIR	SWIR1	SWIR2
Cultivated land	93.71	87.08	106.69	227.27	228.40	178.67
Forest	67.73	53.17	66.42	171.07	173.08	117.86
Grassland	79.80	83.88	117.96	132.67	210.97	161.98
Shrubland	85.29	70.97	84.87	227.77	224.08	156.93
Wetland	73.59	53.18	64.70	194.39	178.76	122.29
Artificial surfaces	110.28	101.14	119.61	192.49	202.36	190.95
Bare land	128.17	144.13	167.41	223.33	271.25	244.67

(a) HLS surface reflectance before HLS bandpass adjustment

Cultivated land	99.21	88.14	105.61	227.01	223.18	176.91
Forest	67.72	54.20	64.75	170.78	167.10	115.17
Grassland	80.49	86.29	104.80	132.07	203.58	161.09
Shrubland	85.08	71.81	83.83	227.81	219.50	155.11
Wetland	71.11	53.70	62.73	194.12	172.32	119.50
Artificial surfaces	118.80	102.47	118.02	191.54	197.63	189.70
Bare land	117.32	143.01	169.64	224.76	270.56	245.05

(b) HLS surface reflectance after HLS bandpass adjustment

Cultivated land	140.72	128.42	159.19	330.86	300.72	240.27
Forest	115.14	99.27	124.58	273.30	246.37	175.73
Grassland	93.70	98.12	180.47	232.43	321.24	256.62
Shrubland	120.13	116.67	138.67	341.05	304.37	213.14
Wetland	114.15	102.81	119.63	287.42	245.28	175.44
Artificial surfaces	145.53	136.93	176.00	286.88	277.37	259.12
Bare land	122.71	164.90	225.93	317.33	360.98	309.30

(c) TOA reflectance

Fig. 7. The reflectance differences (expanded 10,000 times) between Landsat 8 and Sentinel-2 surface reflectance in the HLS product and TOA reflectance for different land cover types. (a) was calculated between L30 and NadirS30, (b) was calculated between L30 and S30, and (c) was calculated between Landsat 8 and Sentinel-2 TOA reflectance.

study area were used to indicate the overall performance of the TRA approach. For convenience, the calculated RMSDs were expanded 10,000 times in magnitude. We divided the time series observations of each individual pixels into two parts for evaluating TRA performance, with 75% randomly selected to build the reflectance adjustment relationship and the remaining 25% used for evaluation. Note that for the algorithm development (e.g., selecting the optimal matching and interpolating methods), we only selected 5,000 pixels randomly (spatially) for each site for efficiency.

One of the key issues using the time-series-based reflectance adjustment approach is whether the spatial patterns and heterogeneity of land surface would be changed by the reflectance adjustment approach, and we evaluated this by calculating the semi-variogram of the adjusted images (Equation (4)).

$$\gamma(h, \Lambda) = \frac{1}{2N} \sum_{i=1}^N (\rho(x_i + h, \Lambda) - \rho(x_i, \Lambda))^2 \quad (4)$$

where, Λ is the band index, $\rho(x_i, \Lambda)$ is the reflectance at the location of x_i , $\rho(x_i + h, \Lambda)$ is the reflectance at a distance of h from x_i , i is the number index, and N is the total counts of reflectance values at the distance of h with all directions. We chose the SWIR1 band to assess the ability of the TRA approach for reserving the spatial patterns of land surface due to its large variation in reflectance values. For each site, the pair of Landsat 8 and Sentinel-2 images acquired close in time, with a high percentage of overlapped clear-sky observations were chosen to calculate the semi-variogram (The acquisition dates of selected Landsat 8 and Sentinel-2 images are given in Table S1). There were up to

3660 × 3660 pixels at a site, and we randomly selected 20,000 clear-sky pixels to represent the whole site for calculating the semi-variogram. If the shape of semi-variograms of the adjusted Sentinel-2 images doesn't change (compared to original Sentinel-2 images), we think this approach has reserved the spatial patterns of land surface.

3. Results

3.1. HLS and TOA reflectance difference

The HLS product used a fixed set of bandpass adjustment parameters (Claverie et al., 2018) to reduce the bandpass differences at the global scale, but there were still observable surface reflectance differences. Fig. 6 illustrates the surface reflectance difference (indicated by mean RMSDs) between matched (within ± 1 day) Landsat 8 and Sentinel-2 observation pairs before (Fig. 6a) and after (Fig. 6b) the HLS bandpass adjustment for six spectral bands at the five sites (a total of 30 band-sites, hereafter we use the term “band-site” to represent one spectral band at one site). We found Fig. 6a and b are very similar, and for some band-sites, the RMSDs even increased after NASA's HLS bandpass adjustment. We also evaluated the RMSDs for different land cover types, and they varied wildly among different land cover types (Fig. 7a and Fig. 7b), which demonstrated the importance of building reflectance adjustment relationship for each individual pixel, instead of sharing the same adjustment relationship for all pixels.

The reflectance differences between Landsat 8 and Sentinel-2 TOA reflectance for six spectral bands were also evaluated by the mean

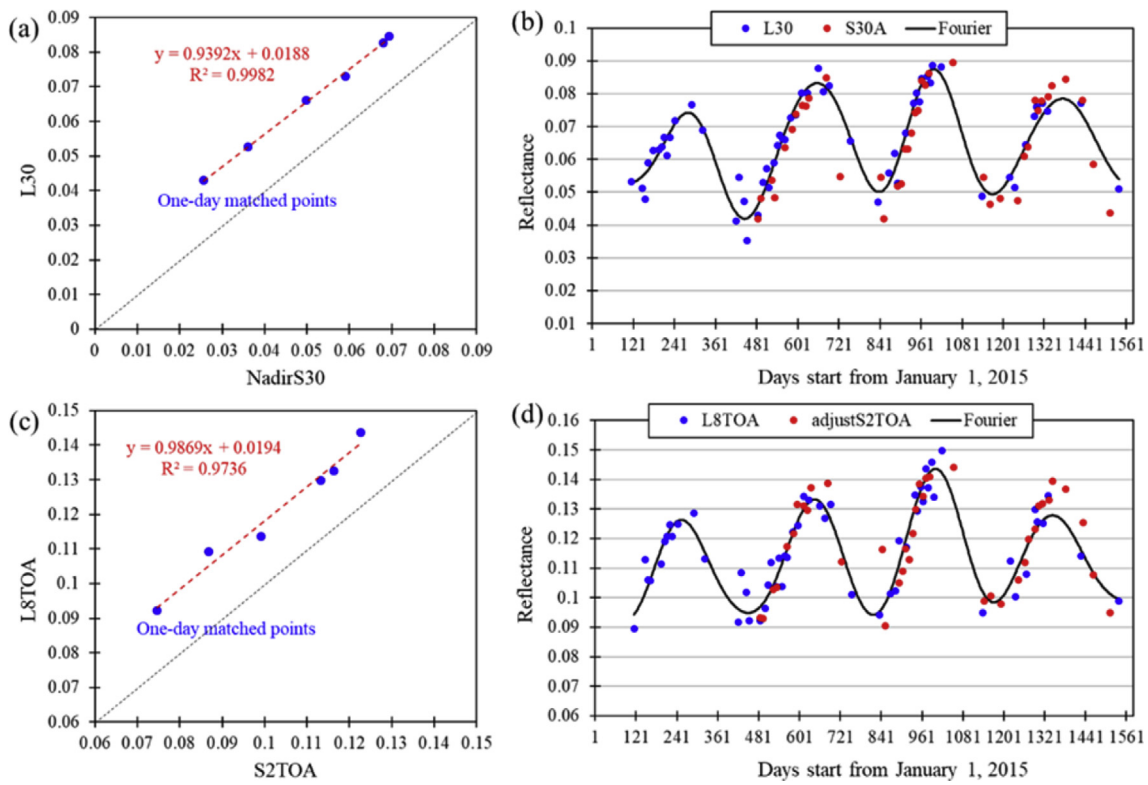


Fig. 8. The generation of reflectance adjustment relationship (a, c) and the reflectance adjustment on the blue band for HLS product (b) and TOA reflectance (d) by the TRA approach for the same pixels in Fig. 1. The black dot lines in (a, c) are 1:1 line. The black lines in (b, d) are the fitted curves of the L30 and L8TOA based on the Fourier approach, respectively. L30: Landsat 8 data in the HLS product; NadirS30: Sentinel-2 surface reflectance before HLS bandpass adjustment; S30A: the adjusted Sentinel-2 surface reflectance; L8TOA: Landsat 8 TOA reflectance; S2TOA: the resampled Sentinel-2 TOA reflectance at 30-m spatial resolution; adjust-S2TOA: the adjusted Sentinel-2 TOA reflectance. (For interpretation of the references to color in this figure legend, the reader is referred to the Web version of this article.)

	Blue	Green	Red	NIR	SWIR1	SWIR2		Blue	Green	Red	NIR	SWIR1	SWIR2
Before	71.61	84.60	98.20	269.86	206.30	149.97		147.17	145.52	168.77	425.78	315.51	199.25
After	42.35	53.62	64.94	182.76	131.47	100.36		88.13	88.36	97.26	263.39	197.93	120.95
Reduce	40.86%	36.63%	33.86%	32.28%	36.27%	33.08%		40.12%	39.28%	42.37%	38.14%	37.27%	39.29%
	DE							DE					
Before	90.33	94.25	135.41	126.70	217.32	168.08		88.00	93.12	191.88	216.74	303.27	247.65
After	41.68	48.61	77.04	90.19	141.90	120.68		40.00	45.79	87.19	113.49	166.76	138.70
Reduce	53.86%	48.43%	43.10%	28.82%	34.70%	28.20%		54.55%	50.83%	54.56%	47.64%	45.01%	43.99%
	SEA							SEA					
Before	92.14	98.00	118.54	160.79	179.21	154.30		146.02	119.85	152.56	225.34	217.01	201.04
After	56.79	59.77	79.65	110.97	111.72	101.15		86.39	78.37	92.56	131.13	123.92	116.77
Reduce	38.36%	39.01%	32.80%	30.99%	37.66%	34.44%		40.84%	34.61%	39.33%	41.81%	42.90%	41.92%
	SHA							SHA					
Before	71.81	79.49	102.51	272.56	263.11	177.14		128.81	123.14	143.90	333.51	304.70	209.31
After	38.11	48.36	61.30	181.76	156.23	109.66		72.81	71.46	78.55	197.57	162.32	111.89
Reduce	46.93%	39.17%	40.21%	33.31%	40.62%	38.10%		43.47%	41.97%	45.42%	40.76%	46.73%	46.55%
	TIF							TIF					
Before	49.94	56.74	67.34	134.92	150.74	106.32		110.72	90.72	119.42	186.97	206.05	158.91
After	30.49	37.14	44.57	100.99	96.86	73.21		58.34	57.74	68.40	120.26	119.51	87.05
Reduce	38.94%	34.54%	33.82%	25.15%	35.74%	31.14%		47.31%	36.35%	42.72%	35.68%	42.00%	45.22%
	TZ							TZ					
Before	75.11	83.69	107.97	174.50	197.44	149.13		114.69	104.00	158.89	245.24	263.28	207.12
After	41.20	48.76	66.57	121.77	125.35	101.48		61.48	60.40	83.14	143.01	148.71	116.33
Reduce	45.15%	41.74%	38.34%	30.22%	36.51%	31.95%		46.40%	41.92%	47.68%	41.68%	43.51%	43.83%
	Average of entire study area							Average of entire study area					
	(a) HLS							(b) TOA					

Fig. 9. The mean RMSDs (expanded 10,000 times) before and after the TRA adjustment and the reduced percentage of mean RMSDs based on the HLS product (a) and TOA reflectance (b) for six spectral bands for all five sites.

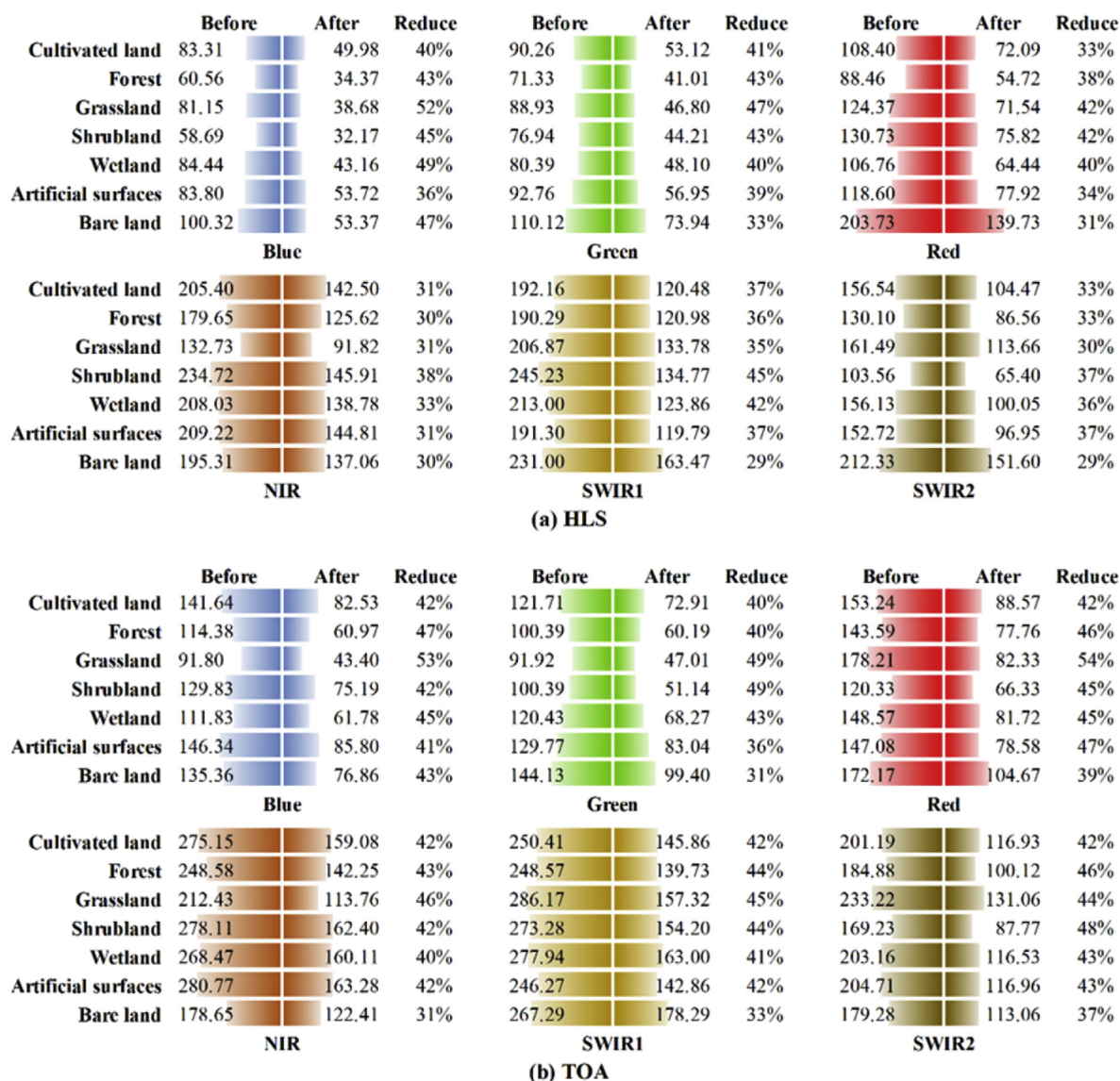


Fig. 10. The reflectance difference before and after the TRA adjustment and the reduced percentages of reflectance difference for different land cover types based on the HLS product (a) and TOA reflectance (b).

RMSDs. Fig. 6c shows the mean RMSDs between Landsat 8 and Sentinel-2 TOA reflectance for six spectral bands at the five sites. Compared to HLS surface reflectance, TOA reflectance generally had a larger reflectance difference for the six spectral bands. The average difference of TOA reflectance across the study area was 1.4–1.7 times the average difference of surface reflectance in the HLS product. These results revealed that atmospheric correction and BRDF correction could reduce part of the reflectance difference between Landsat 8 and Sentinel-2 observations. Similar to HLS surface reflectance, TOA reflectance difference varied largely for different kinds of land cover types (Fig. 7c).

3.2. Reduce HLS and TOA reflectance difference using TRA

The TRA approach can reduce both HLS and TOA reflectance difference between Landsat 8 and Sentinel-2 substantially (Fig. 8). Fig. 8a and b demonstrates the process of building the reflectance adjustment relationship and adjusting the HLS product for the same pixel shown in Fig. 1 based on the TRA approach, respectively. Fig. 9a illustrates the mean RMSDs before and after the TRA adjustment, and the reduced percentage of mean RMSDs based on the HLS product for six spectral bands at the five sites. Note that the mean RMSD before the reflectance

adjustment at each band-site was slightly different from that in Fig. 6b, because the mean RMSD calculated here was only based on the randomly selected 25% of observations. By applying the TRA approach, the reflectance difference in the HLS product reduced 45% for the blue band, 42% for the green band, 38% for the red band, 30% for the NIR band, 37% for the SWIR1 band, and 32% for the SWIR2 band. And the remaining reflectance difference (expanded 10,000 times) was 41.20 for the blue band, 48.76 for the green band, 66.57 for the red band, 121.77 for the NIR band, 125.35 for the SWIR1 band, and 101.48 for the SWIR2 band.

The TOA reflectance difference between Landsat 8 and Sentinel-2 could also be reduced by the TRA approach. Fig. 8c and d presents the process of building the reflectance adjustment relationship and adjusting the TOA reflectance for the same pixel shown in Fig. 1 based on the TRA approach, respectively. Though the built relationship ($R^2 = 0.9736$) was slightly weaker than that of the HLS product ($R^2 = 0.9982$), the TRA approach performed well on reducing the TOA reflectance difference. Fig. 9b shows the mean RMSDs before and after the TRA adjustment on TOA reflectance and the reduced percentage of mean RMSDs for six spectral bands at the five sites. After applying the TRA adjustment, the difference between Landsat 8 and Sentinel-2 TOA

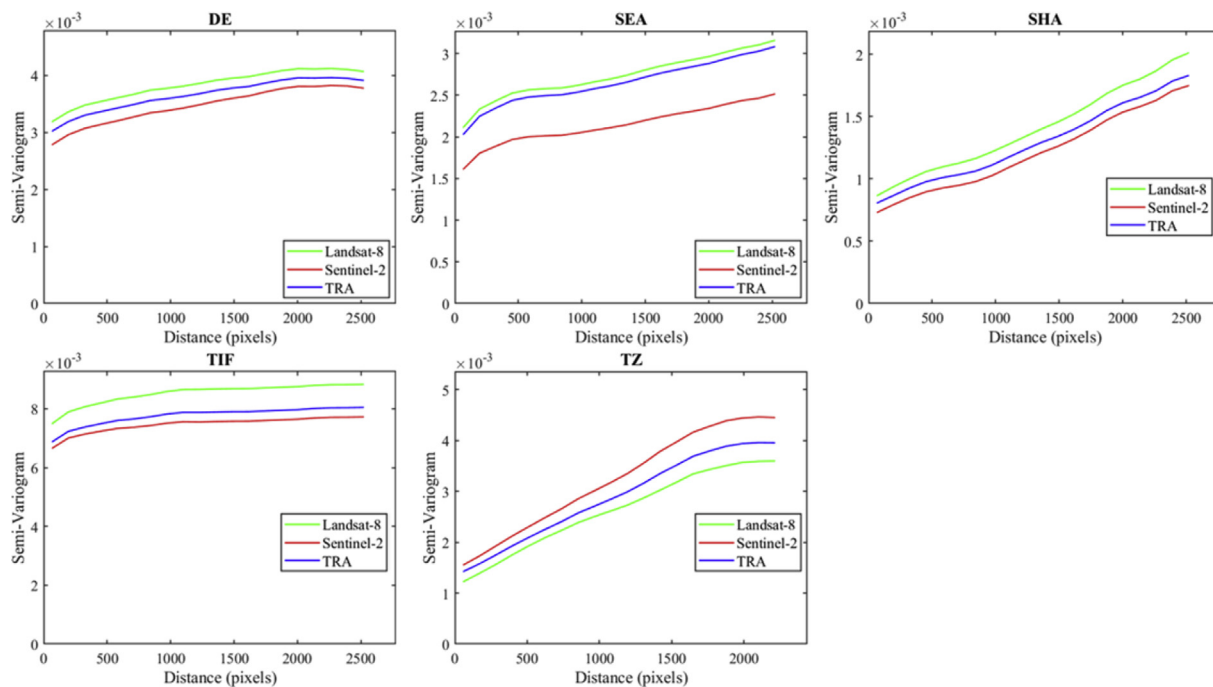


Fig. 11. The semi-variograms calculated from Landsat 8, Sentinel-2, and the adjusted Sentinel-2 images at the SWIR1 band for the five sites.

reflectance reduced 46% for the blue band, 42% for the green band, 48% for the red band, 42% for the NIR band, 44% for the SWIR1 band, and 44% for the SWIR2 band. The reduced percentage of TOA reflectance difference by the TRA approach was up to 12% higher compared with that on the HLS product, suggesting a better performance of reflectance adjustment on TOA reflectance than that on surface reflectance. The remaining TOA reflectance difference after the TRA adjustment was even smaller than the surface reflectance difference in the HLS product without the TRA adjustment.

The reduction of reflectance difference by the TRA approach varied among different land cover types. Fig. 10a shows the reflectance difference before and after the TRA adjustment and the reduced percentages of reflectance difference in the HLS product for different land cover types. Grassland had the largest reduction of reflectance difference in three visible bands (52% for the blue band, 47% for the green band, and 42% for the red band); while in the NIR and SWIR bands, shrubland had the largest reduction of reflectance difference (38% for the NIR band, 45% for the SWIR1 band, and 37% for the SWIR2 band). Artificial surfaces had the smallest reduction of reflectance difference (36%) in the blue band, and bare land had the smallest reduction of reflectance difference in the green (33%), red (31%), NIR (30%), SWIR1 (29%), and SWIR2 (29%) bands. Fig. 10b shows the TOA reflectance difference before and after the TRA adjustment and the reduced percentages of TOA reflectance differences for different land cover types. The patterns of reducing TOA reflectance difference among different land cover types were very similar to that for reducing HLS reflectance difference. These discrepancies in the reflectance differences and the reduction of reflectance differences by the TRA adjustment among different land cover types further confirmed the requirement of time-series-based reflectance adjustment approach for harmonizing Landsat 8 and Sentinel-2 surface reflectance and TOA reflectance.

3.3. Assess TRA's ability to reserve the spatial patterns of land surface

Whether the spatial patterns will be changed is one of the key issues using the time-series-based reflectance adjustment approach. The semi-variogram was used to assess the ability of the TRA approach for

reserving the spatial patterns of land surface. Fig. 11 shows the semi-variograms calculated from Landsat 8, Sentinel-2 and the adjusted Sentinel-2 images in the SWIR1 band at the five sites. The semi-variogram generally increased with the increase of distance at the five sites. Landsat 8 and Sentinel-2 images observed the same land surface and their semi-variograms had the same shapes, but significant offsets were observed between their semi-variograms, indicating that the reflectance differences between these two sensors varied spatially. The semi-variograms derived from Landsat 8 image were higher than that derived from Sentinel-2 image at the DE, SEA, SHA and TIF sites, while it was lower than that of Sentinel-2 at the TZ site which might be explained by the lower SWIR1 band surface reflectance of Landsat 8 than Sentinel-2 at this site. By applying the TRA adjustment, the offsets between the semi-variograms derived from Landsat 8 and Sentinel-2 images decreased at all five sites, and we did not observe any change of the semi-variograms shape. Fig. 12 shows a typical example of the TRA adjustment for the clipped Landsat 8 and Sentinel-2 images (300×300 pixels) at the five sites. The first three columns are the true color composited RGB images derived from Landsat 8 (L30), Sentinel-2 (S30) and the adjusted Sentinel-2 (S30A), and the last two columns are absolute differences in SWIR1 band surface reflectance between L30 and S30 and between L30 and S30A, respectively. The acquisition date of Landsat 8 and Sentinel-2 images and the subregion extent at the five sites were summarized in Table S1. The reflectance differences between Landsat 8 and Sentinel-2 were significantly reduced by the TRA approach, and the spatial patterns and heterogeneity of land surface in Sentinel-2 RGB images kept the same after the TRA adjustment. These results suggested that the TRA approach had the ability to reserve the spatial patterns and heterogeneity of land surface.

4. Discussion

4.1. Evaluate TRA's capability of adjusting future Sentinel-2 images

To evaluate TRA's capability in adjusting future Sentinel-2 images (hereafter referred as to external evaluation), we used the first 75% of observations to build the reflectance adjustment relationship and the last 25% of observations for evaluation. Fig. 13a shows the mean

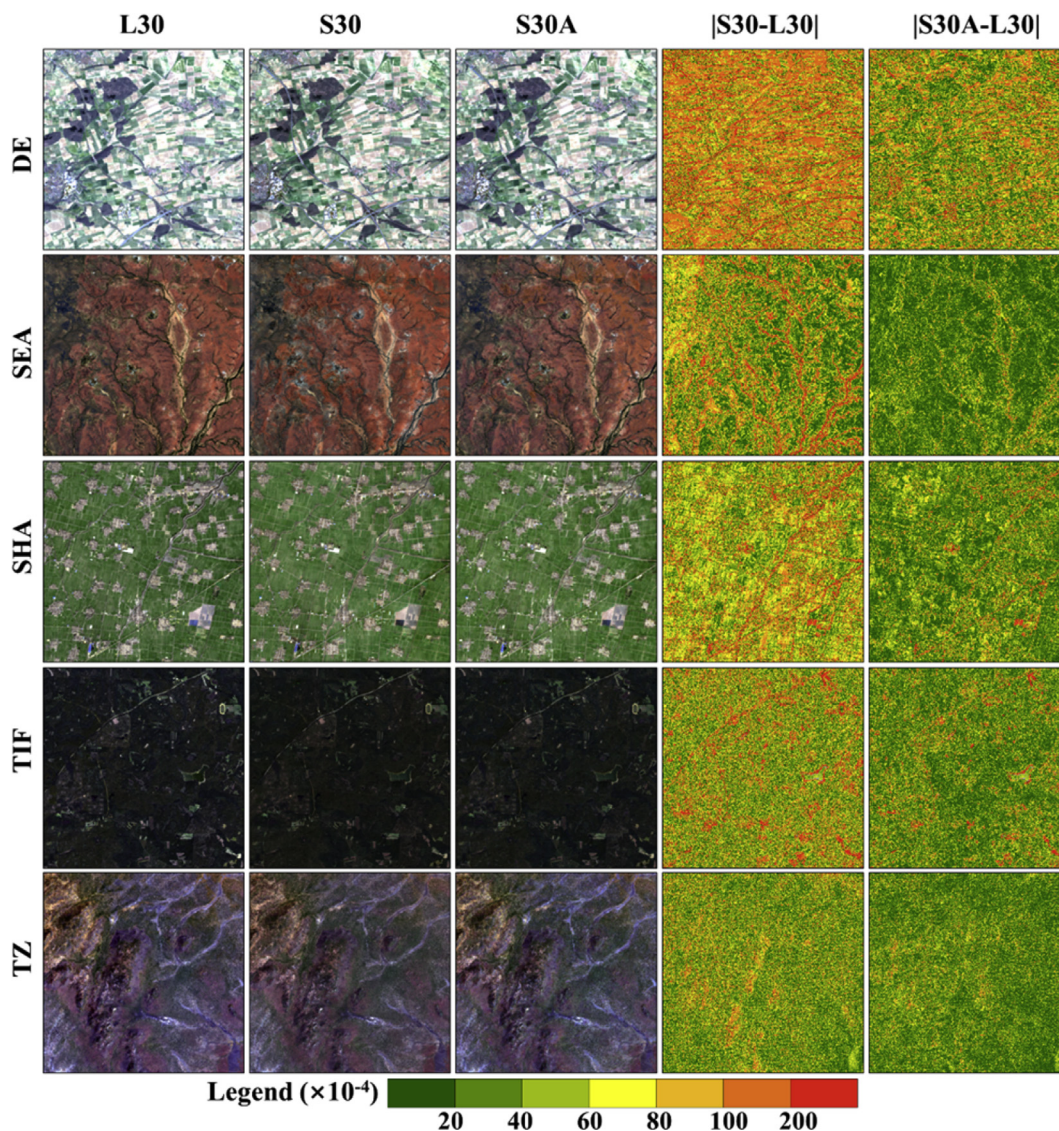


Fig. 12. The true color RGB images of the clipped Landsat 8 observations (L30), the Sentinel-2 observations (S30) and the adjusted Sentinel-2 observations (S30A), and their absolute difference images of the SWIR1 band surface reflectance. “|S30-L30|” is the absolute difference of SWIR1 band surface reflectance between S30 and L30 and “|S30A-L30|” is the absolute difference of SWIR1 band surface reflectance between S30A and L30. (For interpretation of the references to color in this figure legend, the reader is referred to the Web version of this article.)

RMSDs before and after the TRA adjustment and the reduced percentage of mean RMSDs based on the HLS product for the six spectral bands for all five sites. By applying the TRA approach, the reflectance difference in the HLS product reduced 42% for the blue band, 37% for the green band, 38% for the red band, 29% for the NIR band, 35% for the SWIR1 band, and 31% for the SWIR2 band. The reduced percentage of mean RMSDs for the six spectral bands was up to 5% lower than they are evaluated in Section 3.2.

We also evaluated TRA’s capability for adjusting future Sentinel-2 TOA reflectance following the same procedure. Fig. 13b shows the mean RMSDs before and after the TRA adjustment and the reduced percentage of mean RMSDs based on TOA reflectance for the six spectral bands for all five sites. After the TRA adjustment, the difference of TOA reflectance reduced 45% for the blue band, 39% for the green band, 47% for the red band, 40% for the NIR band, 41% for the SWIR1 band, and 42% for the SWIR2 band. The reduced percentage of mean RMSDs for the six spectral bands was up to 3% lower than they are evaluated in Section 3.2. Compared to the external evaluation of the HLS product, the remaining TOA reflectance differences were slightly larger, but the reduced percentage of reflectance difference by the TRA

approach was up to 11% higher.

Both results indicate the generated transformation parameters based on the historical data could be used to adjust future Sentinel-2 images, though the reduction of reflectance difference would be slightly smaller than that using the updated transformation parameters with all data.

4.2. Evaluation of the unmatched Sentinel-2 observations

We evaluated the TRA approach based on matched Landsat 8 and Sentinel-2 observations that are collected within ± 1 day, but this could not provide an evaluation for Landsat 8 and Sentinel-2 observations that are more than ± 1 day apart. To evaluate these unmatched observations, we compared them with the same day optimally interpolated Landsat 8 observations. As interpolation can have large artifact when there is no real observation, we only use the interpolated values that are within the ± 16 days of clear Landsat 8 observations. Fig. S4 shows the mean RMSDs (expanded 10,000 times) before and after the TRA adjustment and the reduced percentage of mean RMSDs for the unmatched Sentinel-2 observations in the HLS product and TOA reflectance. It is obvious that the TRA approach can also reduce

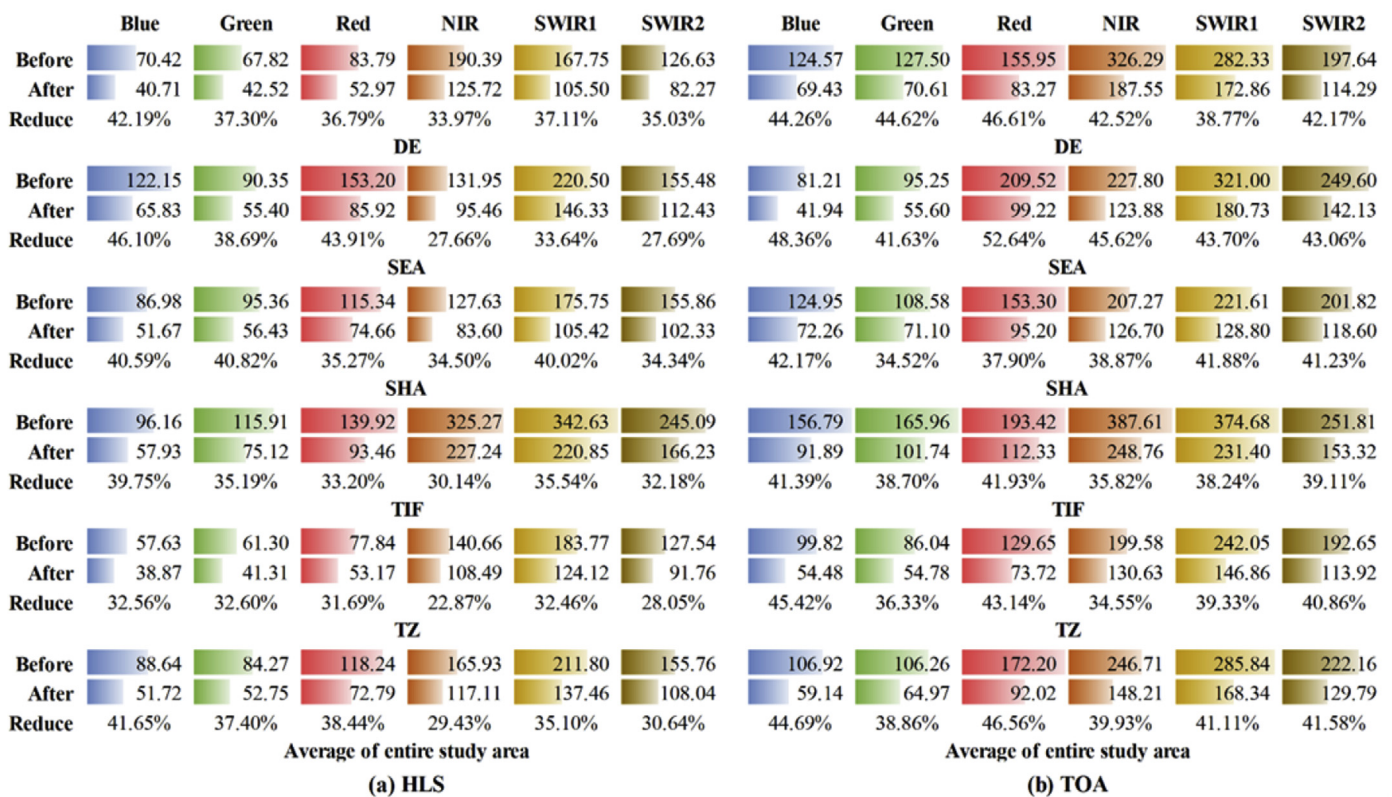


Fig. 13. The mean RMSDs (expanded 10,000 times) before and after the TRA adjustment and the reduced percentage of mean RMSDs based on the HLS V1.4 product (a) and TOA reflectance (b) for six spectral bands for all five sites under the external evaluation.

reflectance differences for all the unmatched observations, though the reduction of reflectance difference was slightly lower (8%) than that on the matched observations, which may contribute both from the artifact of interpolation and changes in land surface.

4.3. The influence of land change on reflectance adjustment

We also evaluated whether the land change would influence the reflectance adjustment. Fig. 14 shows the reflectance difference, the generation of reflectance adjustment relationship, and the reflectance adjustment for a pixel that has undergone change based on the HLS product and the TOA reflectance. The change happened during the time period from May to June 2016 (Fig. 14a and d). Two situations were included in the generation of reflectance adjustment relationship (Fig. 14b and e): one was using all the observations after the change and the other was using all observations. For both surface reflectance and TOA reflectance, the established relationships from all observations were slightly weaker than the built relationship from the observations after disturbance, but the two relationships both performed well on reducing the reflectance difference (Fig. 14c and f). This example suggested that land change had limited impact on the generation of reflectance adjustment relationship. Note that for some ephemeral changes, such as snow observations, they can change land surface within a day, which can have large impacts on the TRA approach. Therefore, we exclude all snow observations for building and applying the reflectance adjustment in the TRA approach.

4.4. The influence of aerosol screening on reflectance adjustment

We also explored the impacts of aerosols on reflectance adjustment. Fig. 14 shows the mean RMSDs before and after the TRA adjustment and the reduced percentage of mean RMSDs based on the HLS product and TOA reflectance after excluding all high aerosol observations. The percentages of pixels that can be adjusted by the TRA approach for each

site after high aerosol screening were shown in Table S3. High aerosol screening decreased the percentage of pixels that can be adjusted from 99.94% to 99.77% at the entire study area, but the reflectance difference in the HLS product was further reduced by 2–4% for the six spectral bands, and the remaining reflectance differences were reduced to 36.13 for the blue band, 42.57 for the green band, 56.89 for the red band, 109.74 for the NIR band, 112.41 for the SWIR1 band, and 89.70 for the SWIR2 band (Fig. 15a). When applying high aerosol screening on TOA reflectance, the reflectance differences could be further reduced by 3–6% (Fig. 15b), and the remaining reflectance differences were comparable to the remaining reflectance differences in the HLS product after the TRA adjustment without high aerosol screening. Therefore, high aerosol screening can further improve the TRA approach, but may also reduce the percentage of pixels that can be adjusted by TRA.

5. Conclusion

This study proposed a time-series-based reflectance adjustment approach (TRA) to reduce the reflectance difference between Landsat 8 and Sentinel-2 surface reflectance from the HLS product and TOA reflectance. The source code is publicly available at <https://github.com/GERSL/TRA>. This TRA approach used the time series of matched Landsat 8 and Sentinel-2 observations to build linear regression models for reflectance adjustment at the pixel level. We evaluated this approach on the NASA harmonized Landsat and Sentinel-2 (HLS) V1.4 surface reflectance product and TOA reflectance with approximately 4 years of temporal coverage at five MGRS tiles. Using this approach, the reflectance difference in the HLS product reduced 45% for the blue band, 42% for the green band, 38% for the red band, 30% for the NIR band, 37% for the SWIR1 band and 32% for the SWIR2 band. The reflectance difference between Landsat 8 and Sentinel-2 TOA reflectance reduced 46% for the blue band, 42% for the green band, 48% for the red band, 42% for the NIR band, 44% for the SWIR1 band, and 44% for the SWIR2 band. The TRA approach was accurate for both matched and

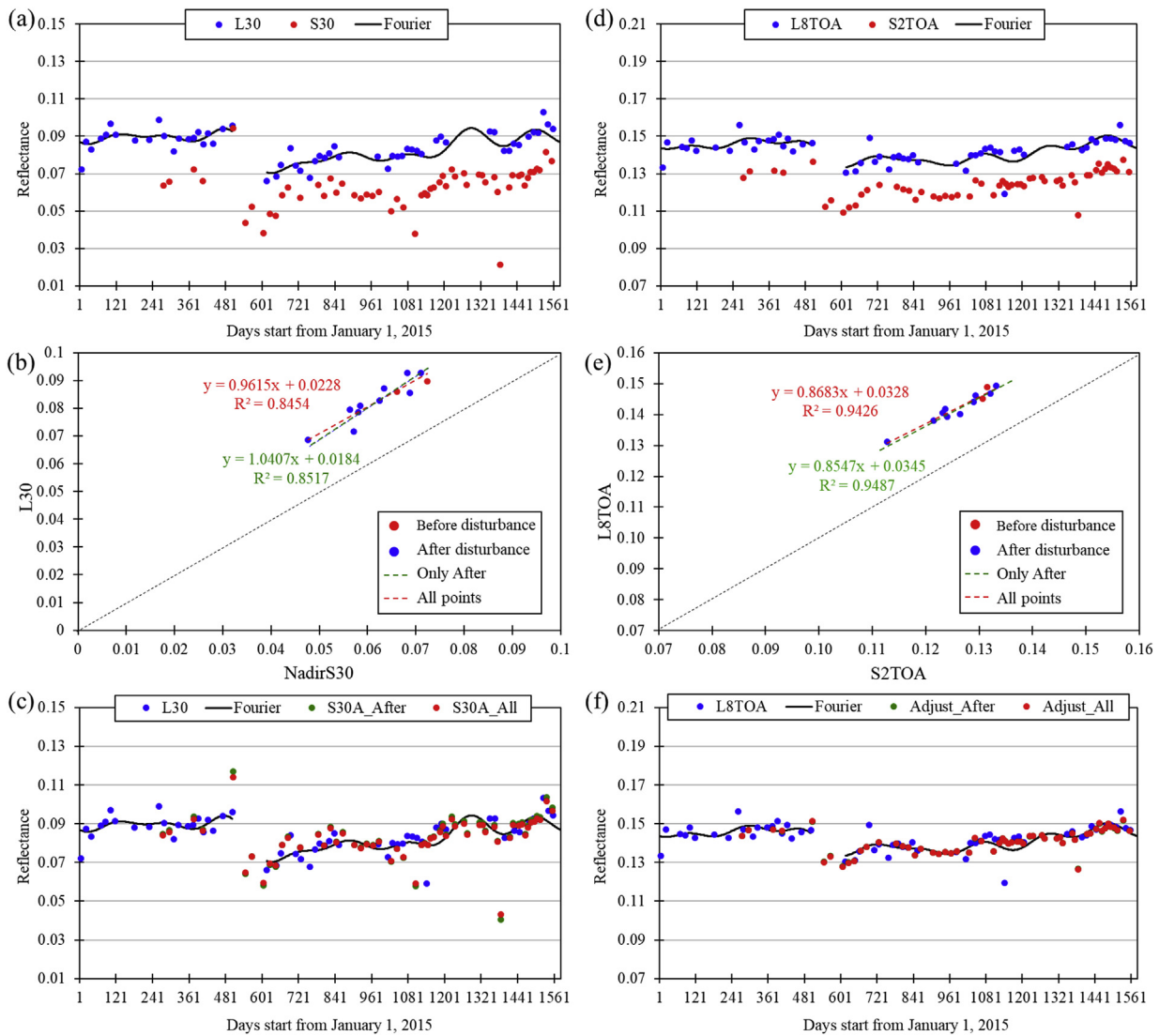


Fig. 14. An example of reflectance difference (a, d), the generation of transformation coefficients (b, e), and the reflectance adjustment (c, f) for blue band based on the HLS product (a–c) and the TOA reflectance (d–f). The black lines are the fitted curves of the L30 and L8TOA based on the Fourier approach, respectively. The invalid observations (cloud, cloud shadow, and snow) were screened by the QA band in the HLS product. L30: Landsat 8 data in the HLS product; S30: Sentinel-2 data in the HLS product at 30-m resolution; NadirS30: Sentinel-2 surface reflectance before the HLS bandpass adjustment; S30A_After: the adjusted Sentinel-2 surface reflectance using the relationship derived from observations after disturbance; S30A_All: the adjusted Sentinel-2 surface reflectance using the relationship derived from all observations; L8TOA: Landsat 8 TOA reflectance; S2TOA: the resampled Sentinel-2 TOA reflectance; Adjust_After: the adjusted Sentinel-2 TOA reflectance using the relationship derived from observations after disturbance; Adjust_All: the adjusted Sentinel-2 TOA reflectance using the relationship derived from all observations. (For interpretation of the references to color in this figure legend, the reader is referred to the Web version of this article.)

unmatched observations, robust to change pixels, and can be applied directly for harmonizing future observations. If high aerosol observations were screened, the reflectance differences in the HLS product could be further reduced by 2–4% and the TOA reflectance differences could be further reduced by 3–6% for the six spectral bands. The reduction of these reflectance differences varies among different land cover types. The TRA approach could also be applicable for improving data consistency between other similar sensors (e.g., Landsat 4, 5, 7, and Sentinel-2A) as long as there is a temporal overlap between them. Compared to the conventional approaches using fixed per-band transformation coefficients, the TRA approach is more complicated, and the performance of TRA could be influenced by persistent cloud covers or rapid land surface changes. Nevertheless, the per-pixel time-series-based character of the TRA approach crosses the limitations of the conventional fixed transformation coefficients approaches and can provide more accurate reflectance adjustment. With more observations accumulated in the future, the percentage of pixels relying on temporal

interpolations and a 3×3 spatial window will be greatly reduced. Moreover, some other spatio-temporal interpolation approaches (Yan and Roy, 2018) considering both spatial and temporal information, can also be tested as possible future improvements.

Acknowledgments

This research was supported by the USGS-NASA Landsat Science Team Program for Toward Near Real-time Monitoring and Characterization of Land Surface Change for the Conterminous US (140G0119C0008). The authors also would like to acknowledge the NASA harmonized Landsat and Sentinel-2 (HLS) data product downloaded from <https://hls.gsfc.nasa.gov/data/> and Landsat 8 and Sentinel-2 TOA reflectance downloaded from Google Earth Engine. The content of this document does not necessarily represent the views or policies of the Department of the Interior, nor does mention of trade names, commercial products or organizations imply endorsement by

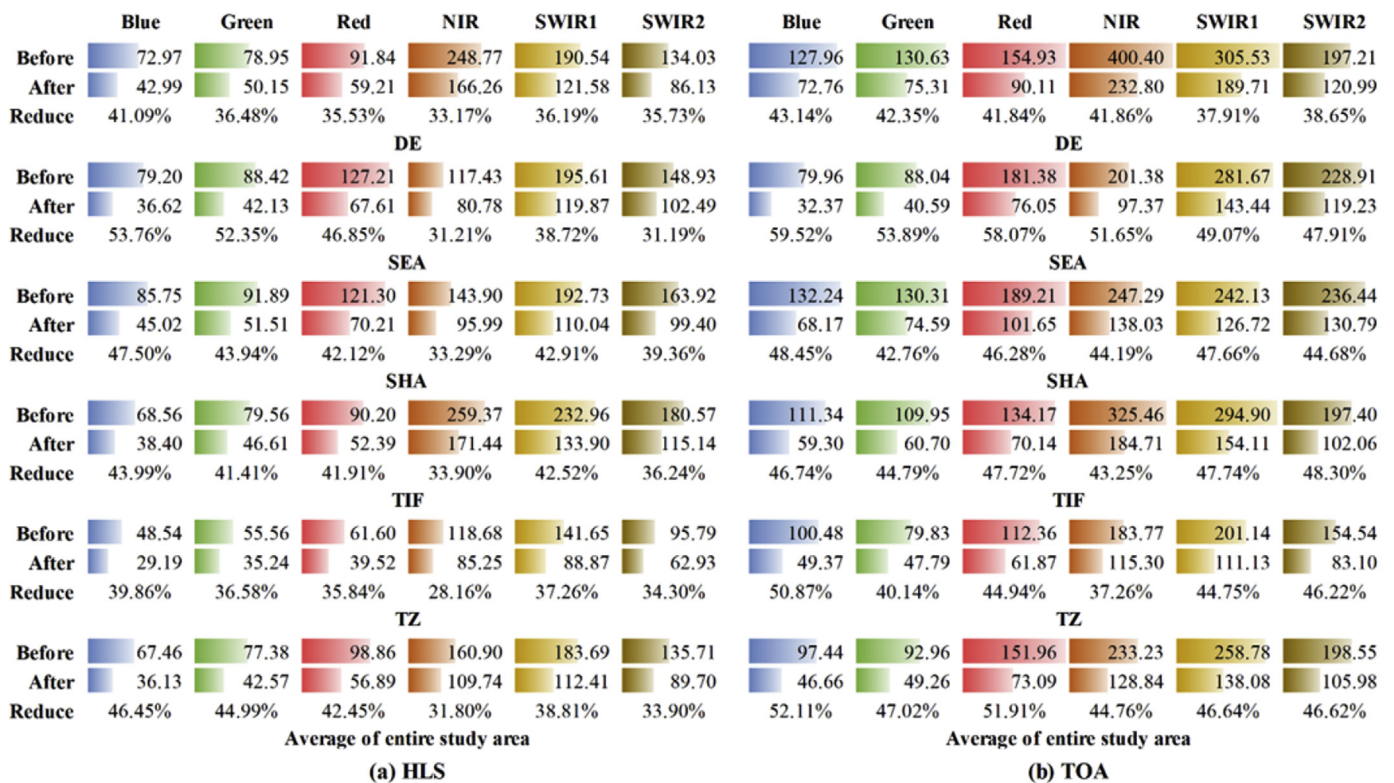


Fig. 15. The mean RMSDs (expanded 10,000 times) before and after the TRA adjustment and the reduced percentage of mean RMSDs based on the HLS product (a) and TOA reflectance (b) with high aerosol screening for six spectral bands at the five sites.

the U.S. Government.

Appendix A. Supplementary data

Supplementary data to this article can be found online at <https://doi.org/10.1016/j.rse.2019.111439>.

References

Chander, G., Mishra, N., Helder, D.L., Aaron, D.B., Angal, A., Choi, T., Xiong, X., Doelling, D.R., 2013. Applications of spectral band adjustment factors (SBAF) for cross-calibration. *IEEE Trans. Geosci. Remote Sens.* 51, 1267–1281.

Chastain, R., Housman, I., Goldstein, J., Finco, M., 2019. Empirical cross sensor comparison of Sentinel-2A and 2B MSI, Landsat-8 OLI, and Landsat-7 ETM+ top of atmosphere spectral characteristics over the conterminous United States. *Remote Sens. Environ.* 221, 274–285.

Chen, J., Jönsson, P., Tamura, M., Gu, Z., Matsushita, B., Eklundh, L., 2004. A simple method for reconstructing a high-quality NDVI time-series data set based on the Savitzky-Golay filter. *Remote Sens. Environ.* 91, 332–344.

Chen, J., Chen, J., Liao, A., Cao, X., Chen, L., Chen, X., He, C., Han, G., Peng, S., Lu, M., Zhang, W., Tong, X., Mills, J., 2015. Global land cover mapping at 30 m resolution: a POK-based operational approach. *ISPRS J. Photogrammetry Remote Sens.* 103, 7–27.

Chen, J.M., Deng, F., Chen, M., 2006. Locally adjusted cubic-spline capping for reconstructing seasonal trajectories of a satellite-derived surface parameter. *IEEE Trans. Geosci. Remote Sens.* 44, 2230–2238.

Claverie, M., Ju, J., Masek, J.G., Dungan, J.L., Vermote, E.F., Roger, J.C., Skakun, S.V., Justice, C., 2018. The Harmonized Landsat and Sentinel-2 surface reflectance data set. *Remote Sens. Environ.* 219, 145–161.

Dash, J., Jegathanan, C., Atkinson, P.M., 2010. The use of MERIS Terrestrial Chlorophyll Index to study spatio-temporal variation in vegetation phenology over India. *Remote Sens. Environ.* 114, 1388–1402.

Defourny, P., Bontemps, S., Bellemans, N., Cara, C., Dedieu, G., Guzzonato, E., Hagolle, O., Inglada, J., Nicola, L., Rabatte, T., Savinaud, M., Udrou, C., Valero, S., Bégué, A., Dejoux, J.-F., El Harti, A., Ezzahar, J., Kussul, N., Labbassi, K., Lebourgeois, V., Miao, Z., Newby, T., Nyamugama, A., Salh, N., Shelestov, A., Simonneaux, V., Traore, P.S., Traore, S.S., Koetz, B., 2019. Near real-time agriculture monitoring at national scale at parcel resolution: performance assessment of the Sen2-Agri automated system in various crop systems around the world. *Remote Sens. Environ.* 221, 551–568.

Drusch, M., Del Bello, U., Carlier, S., Colin, O., Fernandez, V., Gascon, F., Hoersch, B., Isola, C., Laberinti, P., Martimort, P., Meygret, A., Spoto, F., Sy, O., Marchese, F., Bargellini, P., 2012. Sentinel-2: ESA's optical high-resolution mission for GMES

operational services. *Remote Sens. Environ.* 120, 25–36.

Flood, N., 2017. Comparing Sentinel-2A and Landsat 7 and 8 using surface reflectance over Australia. *Remote Sens.* 9, 659.

Gorelick, N., Hancher, M., Dixon, M., Ilyushchenko, S., Thau, D., Moore, R., 2017. Google earth engine: planetary-scale geospatial analysis for everyone. *Remote Sens. Environ.* 202, 18–27.

Hagolle, O., Huc, M., Pascual, D.V., Dedieu, G., 2010. A multi-temporal method for cloud detection, applied to FORMOSAT-2, VENUS, LANDSAT and SENTINEL-2 images. *Remote Sens. Environ.* 114, 1747–1755.

Hansen, M.C., Loveland, T.R., 2012. A review of large area monitoring of land cover change using Landsat data. *Remote Sens. Environ.* 122, 66–74.

Ju, J., Roy, D.P., Vermote, E., Masek, J., Kovalsky, V., 2012. Continental-scale validation of MODIS-based and LEDAPS Landsat ETM+ atmospheric correction methods. *Remote Sens. Environ.* 122, 175–184.

Julien, Y., Sobrino, J.A., 2010. Comparison of cloud-reconstruction methods for time series of composite NDVI data. *Remote Sens. Environ.* 114, 618–625.

Kovalsky, V., Gomez-Dans, J.L., Ju, J., Sun, Q., Zhang, H.K., Huang, H., Li, J., Schaaf, C.B., Roy, D.P., Lewis, P.E., 2016. A general method to normalize Landsat reflectance data to nadir BRDF adjusted reflectance. *Remote Sens. Environ.* 176, 255–271.

Li, J., Roy, D.P., 2017. A global analysis of Sentinel-2a, Sentinel-2b and Landsat-8 data revisit intervals and implications for terrestrial monitoring. *Remote Sens. Environ.* 176, 255–271.

Li, S., Sun, D., Goldberg, M.D., Sjöberg, B., Santek, D., Hoffman, J.P., DeWeese, M., Restrepo, P., Lindsey, S., Holloway, E., 2018. Automatic near real-time flood detection using Suomi-NPP/VIIRS data. *Remote Sens. Environ.* 204, 672–689.

Liu, L., Zhang, X., Yu, Y., Gao, F., Yang, Z., 2018. Real-time monitoring of crop phenology in the Midwestern United States using VIIRS observations. *Remote Sens.* 10, 1540.

Liu, R., Shang, R., Liu, Y., Lu, X., 2017. Global evaluation of gap-filling approaches for seasonal NDVI with considering vegetation growth trajectory, protection of key point, noise resistance and curve stability. *Remote Sens. Environ.* 189, 164–179.

Mandanic, E., Bitelli, G., 2016. Preliminary comparison of sentinel-2 and landsat 8 imagery for a combined use. *Remote Sens.* 8, 1014.

Meroni, M., Fasbender, D., Rembold, F., Atzberger, C., Klisch, A., 2019. Near real-time vegetation anomaly detection with MODIS NDVI: timeliness vs. accuracy and effect of anomaly computation options. *Remote Sens. Environ.* 221, 508–521.

Pahlevan, N., Chittimalli, S.K., Balasubramanian, S.V., Vellucci, V., 2019. Sentinel-2/Landsat-8 product consistency and implications for monitoring aquatic systems. *Remote Sens. Environ.* 220, 19–29.

Pekel, J.F., Vancutsem, C., Bastin, L., Clerici, M., Vanbogaert, E., Bartholomé, E., Defourny, P., 2014. A near real-time water surface detection method based on HSV transformation of MODIS multi-Spectral time series data. *Remote Sens. Environ.* 140, 704–716.

Qiu, S., Lin, Y., Shang, R., Zhang, J., Ma, L., Zhu, Z., 2019. Making landsat time series consistent: evaluating and improving landsat analysis ready data. *Remote Sens.* 11, 51.

- Reiche, J., Hamunyela, E., Verbesselt, J., Hoekman, D., Herold, M., 2018. Improving near-real time deforestation monitoring in tropical dry forests by combining dense Sentinel-1 time series with Landsat and ALOS-2 PALSAR-2. *Remote Sens. Environ.* 204, 147–161.
- Roy, D.P., Wulder, M.A., Loveland, T.R., W, C.E., Allen, R.G., Anderson, M.C., Helder, D., Irons, J.R., Johnson, D.M., Kennedy, R., Scambos, T.A., Schaaf, C.B., Schott, J.R., Sheng, Y., Vermote, E.F., Belward, A.S., Bindschadler, R., Cohen, W.B., Gao, F., Hipple, J.D., Hostert, P., Huntington, J., Justice, C.O., Kilic, A., Kovalskyy, V., Lee, Z.P., Lyburner, L., Masek, J.G., McCorkel, J., Shuai, Y., Trezza, R., Vogelmann, J., Wynne, R.H., Zhu, Z., 2014. Landsat-8: science and product vision for terrestrial global change research. *Remote Sens. Environ.* 145, 154–172.
- Tang, X., Bullock, E.L., Olofsson, P., Estel, S., Woodcock, C.E., 2019. Near real-time monitoring of tropical forest disturbance: new algorithms and assessment framework. *Remote Sens. Environ.* 224, 202–218.
- Wulder, M.A., Loveland, T.R., Roy, D.P., Crawford, C.J., Masek, J.G., Woodcock, C.E., Allen, R.G., Anderson, M.C., Belward, A.S., Cohen, W.B., Dwyer, J., Erb, A., Gao, F., Griffiths, P., Helder, D., Hermosilla, T., Hipple, J.D., Hostert, P., Hughes, M.J., Huntington, J., Johnson, D.M., Kennedy, R., Kilic, A., Li, Z., Lyburner, L., McCorkel, J., Pahlevan, N., Scambos, T.A., Schaaf, C., Schott, J.R., Sheng, Y., Storey, J., Vermote, E., Vogelmann, J., White, J.C., Wynne, R.H., Zhu, Z., 2019. Current status of Landsat program, science, and applications. *Remote Sens. Environ.* 225, 127–147.
- Xin, Q., Olofsson, P., Zhu, Z., Tan, B., Woodcock, C.E., 2013. Toward near real-time monitoring of forest disturbance by fusion of MODIS and Landsat data. *Remote Sens. Environ.* 135, 234–247.
- Yan, L., Roy, D.P., 2018. Large-area gap filling of landsat reflectance time series by spectral-angle-mapper based spatio-temporal similarity (SAMSTS). *Remote Sens.* 10, 609.
- Zhang, H.K., Roy, D.P., Yan, L., Li, Z., Huang, H., Vermote, E., Skakun, S., Roger, J.C., 2018. Characterization of Sentinel-2A and Landsat-8 top of atmosphere, surface, and nadir BRDF adjusted reflectance and NDVI differences. *Remote Sens. Environ.* 215, 482–494.
- Zhu, X., Chen, J., Gao, F., Chen, X., Masek, J.G., 2010. An enhanced spatial and temporal adaptive reflectance fusion model for complex heterogeneous regions. *Remote Sens. Environ.* 114, 2610–2623.
- Zhu, Z., 2017. Change detection using landsat time series: a review of frequencies, pre-processing, algorithms, and applications. *ISPRS J. Photogrammetry Remote Sens.* 130, 370–384.
- Zhu, Z., Wang, S., Woodcock, C.E., 2015. Improvement and expansion of the Fmask algorithm: cloud, cloud shadow, and snow detection for Landsats 4-7, 8, and Sentinel 2 images. *Remote Sens. Environ.* 159, 269–277.
- Zhu, Z., Woodcock, C.E., 2012. Object-based cloud and cloud shadow detection in Landsat imagery. *Remote Sens. Environ.* 118, 83–94.
- Zhu, Z., Wulder, M.A., Roy, D.P., Woodcock, C.E., Hansen, M.C., Radeloff, V.C., Healey, S.P., Schaaf, C., Hostert, P., Strobl, P., Pekel, J.-F., Lyburner, L., Pahlevan, N., Scambos, T.A., 2019. Benefits of the free and open Landsat data policy. *Remote Sens. Environ.* 224, 382–385.